NATIONAL ADVISORY COMMITTEE FOR AERONAUTICS

TECHNICAL NOTE 2927

DEFLECTION OF DELTA WINGS HAVING A CARRY-THROUGH-BAY CHORD SMALLER THAN THE WING ROOT CHORD

By Roger W. Peters and Manuel Stein

Langley Aeronautical Laboratory
Langley Field, Va.

Washington
May 1953

NATIONAL ADVISORY COMMITTEE FOR AERONAUTICS

TECHNICAL NOTE 2927

DEFLECTION OF DELTA WINGS HAVING A CARRY-THROUGH-BAY CHORD SMALLER THAN THE WING ROOT CHORD

By Roger W. Peters and Manuel Stein

SUMMARY

Experimentally determined influence coefficients are presented for the deflection of two solid delta wings - one wing of constant thickness and the other of constant thickness ratio - having a carry-through-bay chord smaller than the wing root chord. A theoretical method of analysis is demonstrated for the constant-thickness wing under tip load, and the theoretical results are compared with the experimental results. The theoretical tip-load deflection for a constant-thickness delta wing elastically supported by a carry-through bay of width 35 percent of the wing root chord is twice as large at the tip as the theoretical tip-load deflection for a similar wing clamped 100 percent of the chord at the root.

INTRODUCTION

Design requirements of delta-wing aircraft may dictate the incorporation of a carry-through-bay chord smaller than the wing root chord. Use of a smaller carry-through-bay chord reduces the bending and torsional stiffness and results, consequently, in increased deflections for a given loading. The purpose of this paper is to present the results of deflection tests of two solid delta wings having a carry-through-bay chord smaller than the wing root chord and to demonstrate a theoretical method of analyzing such combinations of wing and carry-through bay.

Results of deflection tests are presented for two solid delta wings of identical plan form having 55° leading-edge sweep, 10° trailing-edge sweep, and a carry-through-bay chord of approximately 35 percent of the wing root chord. One wing is of constant thickness equal to 3 percent of the wing root chord. The other wing has a hexagonal section with a constant maximum-thickness ratio of 3 percent.

The method of analysis derived in the appendix is based on the theory of reference 1 and differs from that of reference 1 in the derivation and

use of the boundary conditions. The derivation in the appendix is for the special case of a constant-thickness delta wing under tip loading. The equations to be solved may be readily extended from reference 1 to apply to wings of arbitrary shape and loading.

SYMBOLS

a,b,d,e	wing dimensions, in. (see fig. 9)
c	wing root chord, in.
l	distance from root to tip, in.
p	uniform load, lb/sq in.
t	thickness of wing, in.
t_{av}	average thickness of wing, in.
w	deflection, in.
x,y	coordinates, in. (see fig. 9)
D	plate stiffness, $Et^3/12(1 - \mu^2)$, lb-in.
$\bar{D}$	plate stiffness based on average thickness, $Et_{av}^3/12(1 - \mu^2)$, lb-in.
E	Young's modulus of material, lb/sq in.
P	tip load, lb
μ	Poisson's ratio of material
φ_b, φ_w	function of x, coefficient in power series for deflection where subscripts b and w stand for bay and wing, respectively

TEST SPECIMENS AND METHOD OF TESTING

Two solid delta-wing specimens with identical plan form having 55° leading-edge sweep, 10° trailing-edge sweep, and a carry-through-bay chord smaller than the wing root chord (fig. 1) were tested in this investigation. One wing was of constant thickness equal to 3 percent of the wing root chord and was cut from 1-inch-thick 75S-T6 aluminum-alloy

plate; the other wing was of hexagonal section with a constant maximum-thickness ratio equal to 3 percent of the wing root chord and was a casting of aluminum alloy No. 355 heat-treated to the T-61 condition. The specimens were supported by clamping the $1\frac{1}{2}$-inch-square support tabs. (See fig. 2.)

Loads were applied consecutively from the tip to the root at the load stations shown in figure 3. Holes of 13/32-inch diameter were drilled for the loading fixtures as the tests proceeded inward toward the root. All loads were applied symmetrically about the longitudinal center line by a winch supported overhead and were measured by proving-ring dynamometers as shown in figure 4. The tip-load deflections were checked by dead-weight loading.

On the constant-thickness wing, a 1000-pound load was applied to each of the loading stations. On the cast-aluminum wing, however, the load applied varied from only 28 pounds at the tip to a maximum of 400 pounds at the root to avoid exceeding the elastic limit of the cast material.

Deflections were measured by dial indicators located at the deflection stations shown in figure 3. Note that the deflection stations and load stations were coincident except at stations 1 and 16 at the corners of the wing.

RESULTS AND DISCUSSION

The deflection data are presented in the form of influence coefficients in tables 1 and 2. Since there was no appreciable deflection of the support, the deflection data were obtained directly from the gage readings. Each value given in these tables is the average of the two cross-coupling coefficients; for example, the deflection of station 16 resulting from load at station 1 is averaged with the deflection of station 1 resulting from load at station 16. Deviations from the mean are given in parentheses. The influence coefficients for the constant-thickness wing are based on a 1000-pound load. Those coefficients for the constant-thickness-ratio wing are based on a 100-pound load, although the loads used varied from 28 pounds at the tip to 400 pounds at the root.

The tip-load deflection of the 1-inch constant-thickness wing is compared in figure 5 with that computed by the theory derived in reference 1 and extended in the appendix of the present paper. The deflections are plotted in terms of the dimensionless parameter wD/Pl^2. The experimental tip deflections exceed the theoretical values by approximately 15 to 20 percent. One of the reasons for this discrepancy is

that the experiment indicated deflections at the corners of the carry-through bay whereas the theory assumed zero deflection. This deflection is present because the wing is supported at the tabs rather than at the corners of the carry-through bay. The fact that the deflection at one corner of the carry-through bay is different from that at the other corner indicates that there is a twist at the root of the delta wing about an axis normal to the root. If the theoretical values are changed to include this twist (by a rigid-body movement of the wing), the agreement between experiment and theory would be improved over the entire wing. This correction accounts for about one-half the discrepancy at the tip. In addition, a change should be made in the theoretical results, based on these observations of nonzero deflection at the corners of the carry-through bay, to give the correct spanwise slope at the root. No attempt has been made to effect this correction because of the difficulty of obtaining measurements of small slopes very close to the root. If this correction were made, however, experiment and theory would be in even closer agreement.

The influence coefficients of table 1 were used to approximate the deflected surface of the constant-thickness wing for a uniform load. The results of this approximation are shown in figure 6 where the deflections are plotted in terms of the dimensionless parameter wD/pl^4 in which p is the uniform load in pounds per square inch.

The tip-load deflection and the computed uniform-load deflection for the constant-thickness-ratio wing are shown in figures 7(a) and 7(b), respectively, where $w\bar{D}/Pl^2$ and $w\bar{D}/pl^4$ are the dimensionless parameters. In these expressions, $\bar{D}$ is the plate stiffness based on the average thickness of the wing outboard of the root chord line.

The theoretical tip-load deflections obtained in the appendix from the analysis of the constant-thickness delta wing are compared in figure 8 with those obtained from the theory of reference 1 for a constant-thickness delta wing having the same plan form but having its entire root chord clamped. The conclusion is made that removal of 65 percent of the wing root chord of this wing increases the tip deflection for tip load by approximately 100 percent.

CONCLUDING REMARKS

In order to obtain tables of influence coefficients, deflection tests were conducted on two solid, 55°, delta wings - one wing of constant thickness equal to 3 percent of the wing root chord and the other with a constant maximum-thickness ratio equal to 3 percent of the wing root chord - having a carry-through-bay chord smaller than the wing root chord. The

experimental tip-load deflections of the constant-thickness wing exceed those computed by the present theory by approximately 15 to 20 percent at the tip. A great part of this discrepancy can be attributed to the difference between the root support in the experiment and that assumed in the theory.

The theoretical tip-load deflection for a constant-thickness delta wing elastically supported by a carry-through bay of width 35 percent of the wing root chord is twice as large at the tip as the theoretical tip-load deflection for a similar wing clamped 100 percent of the chord at the root.

Langley Aeronautical Laboratory,
National Advisory Committee for Aeronautics,
Langley Field, Va., January 23, 1953.

APPENDIX

THEORETICAL DEFLECTION UNDER TIP LOADS OF A CONSTANT-THICKNESS DELTA WING HAVING A CARRY-THROUGH-BAY CHORD SMALLER THAN THE WING ROOT CHORD

The theory of reference 1 is used in this appendix to study the problem of a solid constant-thickness delta wing having a carry-through-bay chord smaller than the wing root chord and loaded transversely at the tips. The present problem is idealized so that the wing has the plan form shown in figure 9 and is supported by point supports located at the corners of the carry-through bay. In reference 1 the assumption that the chordwise deflections at any spanwise station may be expressed by the first few terms of a power series is used to simplify small-deflection thin-plate theory by means of the principle of minimum potential energy. If the series is limited to the first three terms, as will be done in the present analysis for both the triangular wing and the carry-through bay, that is, if parabolic chordwise deflections are assumed, the following expressions give the transverse deflection:

For the triangular wing,

$$w = \varphi_{w0}(x) + y\varphi_{w1}(x) + y^2\varphi_{w2}(x) \tag{1}$$

and, for the carry-through bay,

$$w = \varphi_{b0}(x) + y\varphi_{b1}(x) + y^2\varphi_{b2}(x) \tag{2}$$

where x and y are the coordinates shown in figure 9.

The potential energy of the system under consideration is

$$\text{Potential energy} = \frac{D}{2}\int\int\left[\left(\frac{\partial^2 w}{\partial x^2}\right)^2 + \left(\frac{\partial^2 w}{\partial y^2}\right)^2 + 2\mu\,\frac{\partial^2 w}{\partial x^2}\,\frac{\partial^2 w}{\partial y^2} + 2(1-\mu)\left(\frac{\partial^2 w}{\partial x\,\partial y}\right)^2\right]dx\,dy - Pw(l,0)$$

where the integral is to be taken over the total area (both the triangular wing and the carry-through bay) with the appropriate values of w being used. Substitution for w from equations (1) and (2) gives

$$\text{Potential energy} = \frac{1}{2}\int_{-b}^{0}\left\{a_{b1}\left(\varphi_{b0}''\right)^2 + 2a_{b2}\varphi_{b0}''\varphi_{b1}'' + a_{b3}\left[\left(\varphi_{b1}''\right)^2 + 2\varphi_{b0}''\varphi_{b2}''\right] + 2a_{b4}\varphi_{b1}''\varphi_{b2}'' + a_{b5}\left(\varphi_{b2}''\right)^2 + 4a_{b1}\varphi_{b2}^2 + 4\mu\left(a_{b1}\varphi_{b0}'' + a_{b2}\varphi_{b1}'' + a_{b3}\varphi_{b2}''\right)\varphi_{b2} + 2(1-\mu)\left[a_{b1}\left(\varphi_{b1}'\right)^2 + 4a_{b2}\varphi_{b1}'\varphi_{b2}' + 4a_{b3}\left(\varphi_{b2}'\right)^2\right]\right\}dx + \frac{1}{2}\int_{0}^{l}\left\{a_{w1}\left(\varphi_{w0}''\right)^2 + 2a_{w2}\varphi_{w0}''\varphi_{w1}'' + \cdots\right\}dx - P\varphi_{w0}(l)$$

where

$$a_{bn} = D\,\frac{1}{n}\left[(a+d)^n - d^n\right]$$

$$a_{wn} = D\,\frac{1}{n}\left[(c+e)^n - e^n\right]\left(1 - \frac{x}{l}\right)^n$$

and the primes denote differentiation with respect to x.

Minimization of the potential energy by means of the calculus of variations gives

$$\delta(\text{Potential energy}) = 0$$

$$= \int_{-b}^{0} \Big\{ a_{b1}\varphi_{b0}''\delta\varphi_{b0}'' + a_{b2}\left(\varphi_{b0}''\delta\varphi_{b1}'' + \varphi_{b1}''\delta\varphi_{b0}''\right) +$$

$$a_{b3}\left(\varphi_{b1}''\delta\varphi_{b1}'' + \varphi_{b0}''\delta\varphi_{b2}'' + \varphi_{b2}''\delta\varphi_{b0}''\right) +$$

$$a_{b4}\left(\varphi_{b1}''\delta\varphi_{b2}'' + \varphi_{b2}''\delta\varphi_{b1}''\right) + a_{b5}\varphi_{b2}''\delta\varphi_{b2}'' +$$

$$4a_{b1}\varphi_{b2}\delta\varphi_{b2} + 2\mu\Big[\left(a_{b1}\varphi_{b0}'' + a_{b2}\varphi_{b1}'' + a_{b3}\varphi_{b2}''\right)\delta\varphi_{b2} +$$

$$\varphi_{b2}\left(a_{b1}\delta\varphi_{b0}'' + a_{b2}\delta\varphi_{b1}'' + a_{b3}\delta\varphi_{b2}''\right)\Big] +$$

$$2(1-\mu)\Big[a_{b1}\varphi_{b1}'\delta\varphi_{b1}' + 2a_{b2}\left(\varphi_{b1}'\delta\varphi_{b2}' +$$

$$\varphi_{b2}'\delta\varphi_{b1}'\right) + 4a_{b3}\varphi_{b2}'\delta\varphi_{b2}'\Big]\Big\}\,dx +$$

$$\int_{0}^{l} \Big\{ a_{w1}\varphi_{w0}''\delta\varphi_{w0}'' + a_{w2}\left(\varphi_{w0}''\delta\varphi_{w1}'' + \ldots\right)\Big\}dx -$$

$$P\delta\varphi_{w0}(l)$$

Integrating by parts and collecting terms results in

$$0 = \int_{-b}^{0} \left\{ M_{b0}''\delta\varphi_{b0} + V_{b1}'\delta\varphi_{b1} + \left[V_{b2}' + 2\mu M_{b0} + 4(1 - \mu^2)a_{b1}\varphi_{b2} \right]\delta\varphi_{b2} \right\} dx +$$

$$\int_{0}^{l} \left\{ M_{w0}''\delta\varphi_{w0} + V_{w1}'\delta\varphi_{w1} + \left[V_{w2}' + 2\mu M_{w0} + 4(1 - \mu^2)a_{w1}\varphi_{w1} \right]\delta\varphi_{w2} \right\} dx +$$

$$\left(M_{b0}\delta\varphi_{b0}' + M_{b1}\delta\varphi_{b1}' + M_{b2}\delta\varphi_{b2}' - V_{b0}\delta\varphi_{b0} - V_{b1}\delta\varphi_{b1} - V_{b2}\delta\varphi_{b2} \right)_{-b}^{0} +$$

$$\left(M_{w0}\delta\varphi_{w0}' + M_{w1}\delta\varphi_{w1}' + M_{w2}\delta\varphi_{w2}' - V_{w0}\delta\varphi_{w0} - V_{w1}\delta\varphi_{w1} - V_{w2}\delta\varphi_{w2} \right)_{0}^{l} -$$

$$P\delta\varphi_{w0}(l) \tag{3}$$

where

$$M_{bn} = a_{b(n+1)}\varphi_{b0}'' + a_{b(n+2)}\varphi_{b1}'' + a_{b(n+3)}\varphi_{b2}'' + 2\mu a_{b(n+1)}\varphi_{b2}$$

$$V_{bn} = M_{bn}' - 2(1 - \mu)n\left[a_{bn}\varphi_{b1}' + 2a_{b(n+1)}\varphi_{b2}' \right]$$

and similarly for M_{wn} and V_{wn}.

Equation (3) must hold for all admissible variations in w - that is, all variations that satisfy conditions of symmetry, continuity, and constraint. In terms of the φ's, these boundary conditions are as follows:

Symmetry at $x = -b$,

$$\varphi_{b0}'(-b) = \varphi_{b1}'(-b) = \varphi_{b2}'(-b) = 0 \tag{4}$$

continuity at $x = 0$,

$$\varphi_{b0}(0) = \varphi_{w0}(0) \qquad \varphi_{b1}(0) = \varphi_{w1}(0) \qquad \varphi_{b2}(0) = \varphi_{w2}(0) \tag{5}$$

$$\varphi_{b0}'(0) = \varphi_{w0}'(0) \qquad \varphi_{b1}'(0) = \varphi_{w1}'(0) \qquad \varphi_{b2}'(0) = \varphi_{w2}'(0) \tag{6}$$

and zero deflection at $x = 0$; $y = d$, $y = d + a$

$$\left(\varphi_{w0} + d\varphi_{w1} + d^2\varphi_{w2}\right)_{x=0} = 0 \tag{7}$$

$$\left[\varphi_{w0} + (d + a)\varphi_{w1} + (d + a)^2\varphi_{w2}\right]_{x=0} = 0 \tag{8}$$

Since the variation of the φ's is entirely arbitrary in the interior of the triangular wing and of the carry-through bay, it follows from equation (3) that the following differential equations hold

$$M_{b0}'' = 0 \tag{9}$$

$$V_{b1}' = 0 \tag{10}$$

$$V_{b2}' + 2\mu M_{b0} + 4(1 - \mu^2)a_{b1}\varphi_{b2} = 0 \tag{11}$$

$$M_{w0}'' = 0 \tag{12}$$

$$V_{w1}' = 0 \tag{13}$$

$$V_{w2}' + 2\mu M_{w0} + 4(1 - \mu^2)a_{w1}\varphi_{w2} = 0 \tag{14}$$

Since $\delta\varphi_{b0}$, $\delta\varphi_{b1}$, and $\delta\varphi_{b2}$ are arbitrary at $x = -b$, the natural boundary conditions are found to be

$$V_{b0}(-b) = V_{b1}(-b) = V_{b2}(-b) = 0 \tag{15}$$

Since $\delta\varphi_{w0}$, $\delta\varphi_{w1}$, $\delta\varphi_{w2}$, $\delta\varphi_{w0}'$, $\delta\varphi_{w1}'$, and $\delta\varphi_{w2}'$ are arbitrary at $x = l$,

$$V_{w0}(l) = -P \qquad V_{w1}(l) = V_{w2}(l) = 0 \tag{16}$$

$$M_{w0}(l) = M_{w1}(l) = M_{w2}(l) = 0 \tag{17}$$

Since $\delta\varphi_{b0}' = \delta\varphi_{w0}'$, $\delta\varphi_{b1}' = \delta\varphi_{w1}'$, and $\delta\varphi_{b2}' = \delta\varphi_{w2}'$ at $x = 0$,

$$M_{b0}(0) = M_{w0}(0) \qquad M_{b1}(0) = M_{w1}(0) \qquad M_{b2}(0) = M_{w2}(0) \tag{18}$$

By virtue of equations (4), (6), and (9) to (18), equation (3) has now been reduced to

$$\left[V_{b0}\delta\varphi_{b0} + V_{b1}\delta\varphi_{b1} + V_{b2}\delta\varphi_{b2} - \left(V_{w0}\delta\varphi_{w0} + V_{w1}\delta\varphi_{w1} + V_{w2}\delta\varphi_{w2}\right)\right]_{x=0} = 0$$

By using equation (5), this relation becomes

$$\left[(V_{b0} - V_{w0})\delta\varphi_{w0} + (V_{b1} - V_{w1})\delta\varphi_{w1} + (V_{b2} - V_{w2})\delta\varphi_{w2}\right]_{x=0} = 0 \tag{19}$$

This equation must be satisfied for all variations of $\delta\varphi_{w0}$, $\delta\varphi_{w1}$, and $\delta\varphi_{w2}$ that satisfy conditions (7) and (8). Thus, elimination of the $\delta\varphi$'s from equation (19) and from conditions (7) and (8) (with the $\delta\varphi$'s replacing the φ's) gives

$$\left[d(d + a)V_{b0} - (2d + a)V_{b1} + V_{b2}\right]_{x=0} = \left[d(d + a)V_{w0} - (2d + a)V_{w1} + V_{w2}\right]_{x=0} \tag{20}$$

Equations (4) to (8), (15) to (18), and (20) constitute the complete set of 24 boundary conditions that are required for the solution of the six simultaneous fourth-order differential equations (9) to (14).

The differential equations (12) to (14) may be solved for the triangular wing portion in a manner similar to that presented in appendix B of reference 1. Substitution for the unknown of general solutions in the form $\left(1 - \frac{x}{l}\right)^{\gamma}$ leads to the following characteristic equation from which γ may be determined:

$$\gamma^6 - 6\left(16\lambda_1^2 + 1\right)\gamma^4 + \left[320\left(4 + \frac{1 + \mu}{1 - \mu}\right)\lambda_1^4 + 480(1 + 2\epsilon)\lambda_1^2 + 9\right]\gamma^2 -$$

$$4\left[1280\,\frac{1 + \mu}{1 - \mu}\,\lambda_1^6 + 80\left(4 + \frac{1 + \mu}{1 - \mu}\right)\lambda_1^4 + 96\left(1 + \frac{5}{2}\,\epsilon\right)\lambda_1^2 + 1\right] = 0$$

where

$$\lambda_1 = \frac{l}{c}\sqrt{\frac{3}{2}(1 - \mu)}$$

and

$$\epsilon = \left(\frac{e}{c}\right)^2 + \frac{e}{c}$$

The differential equations (9) to (11) may be solved for the carry-through bay by taking general solutions of the form $e^{-\delta\frac{x}{b}}$. Substitution of this expression for the unknown in the differential equations leads to the following characteristic equation from which δ may be determined:

$$\left(\delta^2 - 16\lambda_2^2\right)\left(\delta^4 + 80\lambda_2^2\delta^2 + 320\,\frac{1 + \mu}{1 - \mu}\,\lambda_2^2\right) = 0$$

where

$$\lambda_2 = \frac{b}{a}\sqrt{\frac{3}{2}(1 - \mu)}$$

After extensive manipulation, the coefficients in equations (1) and (2) for the particular wing under consideration are found to be as follows:

For the triangular wing,

$$\frac{\varphi_{w0}D}{Pl^2} = 0.050037x_1^{3.0235} + 0.0098970x_1^{5.8872} - 0.091550x_1^{7.5119} + 0.48972x_1^{2} - 2.9746x_1 + 1.6705$$

$$\frac{\varphi_{w1}D}{Pl} = -0.28224x_1^{2.0235} - 0.26284x_1^{4.8872} + 0.47833x_1^{6.5119} + 0.93032x_1 - 1.1424$$

$$\frac{\varphi_{w2}D}{P} = 0.25064x_1^{1.0235} + 0.40185x_1^{3.8872} - 0.46925x_1^{5.5119} - 0.026679$$

where

$$x_1 = 1 - \frac{x}{l}$$

and, for the carry-through bay,

$$\frac{\varphi_{b0}D}{Pl^2} = -0.095452\cosh\left(2.4548\frac{x}{b}\right) + 0.51484\cosh\left(0.84621\frac{x}{b}\right) + 0.095228\cosh\left(1.1612\frac{x}{b}\right) - 0.094054\sinh\left(2.4548\frac{x}{b}\right) + 0.35477\sinh\left(0.84621\frac{x}{b}\right) + 0.078223\sinh\left(1.1612\frac{x}{b}\right) + 0.019590\frac{x^2}{b^2} + 0.039181\frac{x}{b} - 0.39795$$

$$\frac{\varphi_{b1}D}{Pl} = 0.21915 \cosh\left(2.4548 \frac{x}{b}\right) - 1.2002 \cosh\left(0.84621 \frac{x}{b}\right) -$$

$$0.10692 \cosh\left(1.1612 \frac{x}{b}\right) + 0.21593 \sinh\left(2.4548 \frac{x}{b}\right) -$$

$$0.82703 \sinh\left(0.84621 \frac{x}{b}\right) - 0.087831 \sinh\left(1.1612 \frac{x}{b}\right) + 0.80911$$

$$\frac{\varphi_{b2}D}{P} = -0.12303 \cosh\left(2.4548 \frac{x}{b}\right) + 0.67381 \cosh\left(0.84621 \frac{x}{b}\right) -$$

$$0.12123 \sinh\left(2.4548 \frac{x}{b}\right) + 0.46431 \sinh\left(0.84621 \frac{x}{b}\right) - 0.39422$$

From these equations for the coefficients and from equations (1) and (2), the deflections at any point can be found. The theoretical deflections of the triangular wing are shown in figure 5 where they are compared with those found by experiment.

REFERENCE

1. Stein, Manuel, Anderson, J. Edward, and Hedgepeth, John M.: Deflection and Stress Analysis of Thin Solid Wings of Arbitrary Plan Form With Particular Reference to Delta Wings. NACA TN 2621, 1952.

TABLE 1.- EXPERIMENTAL INFLUENCE COEFFICIENTS FOR CONSTANT-THICKNESS DELTA WING

[Deflections are in inches per 1000 pounds]

Load stations	Deflection stations (a)															
	1	2	3	4	5	6	7	8	9	10	11	12	13	14	15	16
1	1.402	(-0.009) 1.041	(-0.019) .796	(-0.008) .700	(-0.006) .490	(-0.011) .299	0.404	(-0.004) .286	(-0.003) .171	(-0.001) .090	(-0.004) .043	(-0.003) .169	0.030	(-0.001) .013	0.000	(-0.004) -.026
2	(.009) 1.041	.831	(-.008) .616	(-.002) .580	(-.004) .392	(-.006) .228	.358	(-.002) .243	(-.001) .139	(-.001) .068	(-.002) .028	(-.003) .170	(.001) .025	(-.001) .009	(-.001) .000	(-.003) -.019
3	(.020) .796	(.009) .616	.528	(.003) .424	(.002) .326	(-.004) .222	(.005) .240	(.001) .180	.120	.078	(-.003) .040	(.008) .084	.020	.012	(-.001) .002	(-.004) -.020
4	(.008) .700	(.002) .580	(-.002) .424	.459	(-.004) .286	(-.006) .150	(.002) .304	(-.001) .197	(-.001) .104	.042	(-.001) .012	(-.001) .172	.021	.003	(-.001) -.001	(-.001) -.013
5	(.009) .490	(.004) .392	(-.002) .326	(.003) .286	.224	(-.003) .144	(-.001) .181	(-.001) .132	.083	.047	(-.001) .084	(-.003) .068	(-.001) .016	.007	.000	(-.002) -.013
6	(.011) .299	(.007) .228	(.004) .222	(.006) .150	(.004) .144	.138	(.004) .075	(.002) .070	(.001) .063	.052	(-.001) .037	(.008) .004	(.001) .009	.011	.003	(-.002) -.014
7	.404	.358	(-.006) .240	(-.001) .304	(.001) .181	(-.004) .075	.247	(-.002) .150	(-.001) .066	.017	(-.001) -.003	(-.001) .178	(-.001) .017	-.001	-.002	(-.001) -.004
8	(.003) .286	(.003) .243	(-.002) .180	(.001) .197	(.001) .132	(-.002) .070	(.002) .150	.102	.053	.021	(-.001) .006	(-.001) .100	(.001) .012	.001	-.001	(-.001) -.005
9	(.002) .171	(.001) .139	.120	.104	.083	(-.001) .063	(.002) .066	.053	.039	.024	.013	(-.002) .038	.008	.004	.000	(-.001) -.006
10	(.001) .090	(.001) .068	(.001) .072	.042	.047	.052	(.001) .017	(-.001) .021	(.001) .024	.027	(-.001) .022	(-.001) -.007	.004	.007	.002	(-.001) -.007
11	(.004) .043	(.001) .028	(.002) .040	(.002) .012	(.002) .024	(.002) .037	-.003	.006	(.001) .013	(.001) .022	.029	(-.001) -.018	.001	.007	.006	(-.001) -.002
12	(.003) .169	(.003) .170	(-.001) .064	(.002) .172	(.002) .082	(-.001) .004	.178	(.002) .100	(.001) .032	(.001) -.007	-.018	.184	.013	-.006	(-.001) -.002	.002
13	(.001) .030	.025	.020	(.001) .021	.016	(-.001) .009	(.001) .017	.012	.008	.004	.001	.013	.004	.001	.000	-.001
14	(.001) .013	.009	(.001) .012	.003	.007	(-.001) .011	-.001	(.001) .001	.004	.007	.007	-.006	.001	.004	.001	-.004
15	.000	.000	.002	(.001) -.001	.000	.003	-.002	(.001) -.001	.000	.002	(.001) .006	(.001) -.002	.000	.001	.002	(.001) .009
16	(.003) -.026	(.003) -.019	(.003) -.020	(.001) -.013	(.001) -.013	(.001) -.014	(.001) -.004	(.001) -.006	-.006	(.001) -.007	(.002) -.002	.002	-.001	-.004	(-.001) .009	.085

[a] Values in parentheses are deviations from the mean value.

NACA

TABLE 2.- EXPERIMENTAL INFLUENCE COEFFICIENTS FOR CONSTANT-THICKNESS-RATIO DELTA WING

[Deflections are in inches per 100 pounds]

Load stations	Deflection stations (a)															
	1	2	3	4	5	6	7	8	9	10	11	12	13	14	15	16
1	1.637	(-0.017) .608	(-0.007) .265	(-0.006) .190	(-0.002) .116	0.066	(-0.001) .074	(-0.003) .051	(-0.002) .029	(-0.001) .011	(0.001) .001	0.020	(-0.002) .002	0.000	0.000	0.000
2	(.016) .608	.398	.183	(-.003) .166	.092	(-.001) .040	(-.001) .069	.046	.025	.008	.001	(-.001) .023	(-.002) .002	.000	.000	.000
3	(.007) .265	.183	.152	(.002) .099	(.001) .074	.041	(.001) .042	(.001) .038	.021	.010	.003	(.001) .009	(-.001) .001	(-.001) .001	.000	-.001
4	(.006) .190	(.004) .166	(-.003) .099	.163	(-.001) .063	(-.001) .023	.066	(-.001) .040	(-.001) .018	.005	.000	.027	.003	.000	.000	.000
5	(.002) .116	.092	(-.002) .074	(.001) .063	.047	.025	.034	.024	.014	(.001) .006	.002	(-.001) .012	.002	.000	.000	-.001
6	.055	.040	.041	(.001) .023	(.001) .025	.028	(.001) .009	.010	.010	.008	.004	(.001) -.002	.001	.001	.000	-.002
7	(.002) .074	(.001) .069	(-.001) .042	(.001) .066	.034	.009	.082	.031	.011	(.001) .001	-.001	.036	.002	.000	.000	.001
8	(.003) .051	.046	.032	.040	.024	.010	.031	.018	.009	(.001) .002	.000	.019	.002	.000	.000	.000
9	(.001) .029	(-.001) .025	(-.001) .021	.018	(.001) .014	.010	.011	.009	.007	.003	.001	.006	.001	.000	.000	.000
10	.011	.008	.010	.006	.006	.008	.001	.002	.003	.004	.003	-.001	.000	(-.001) .001	.000	-.001
11	(-.001) .001	.001	.003	.000	.002	(-.001) .004	-.001	.000	.001	.003	.005	-.002	.000	(-.001) .001	.000	-.001
12	.020	.023	.009	(.001) .027	.012	-.002	.036	.019	.005	(-.001) -.001	-.002	.072	.002	-.001	.000	.001
13	(.002) .002	(.002) .002	(.002) .001	.003	.002	.001	.002	.002	.001	(-.001) .000	.000	.002	.001	.000	.000	.000
14	(.001) .000	(.001) .000	(.001) .001	.000	(.001) .000	.001	.000	.000	.000	.001	.001	-.001	.000	.001	.000	(-.001) .000
15	.000	.000	.000	.000	.000	.000	.000	.000	.000	.000	.000	.000	.000	.000	.000	(.001) .000
16	.000	.000	-.001	.000	-.001	-.002	.001	.000	.000	-.001	-.001	.001	.000	.000	.000	.047

[a]Values in parentheses are deviations from the mean value.

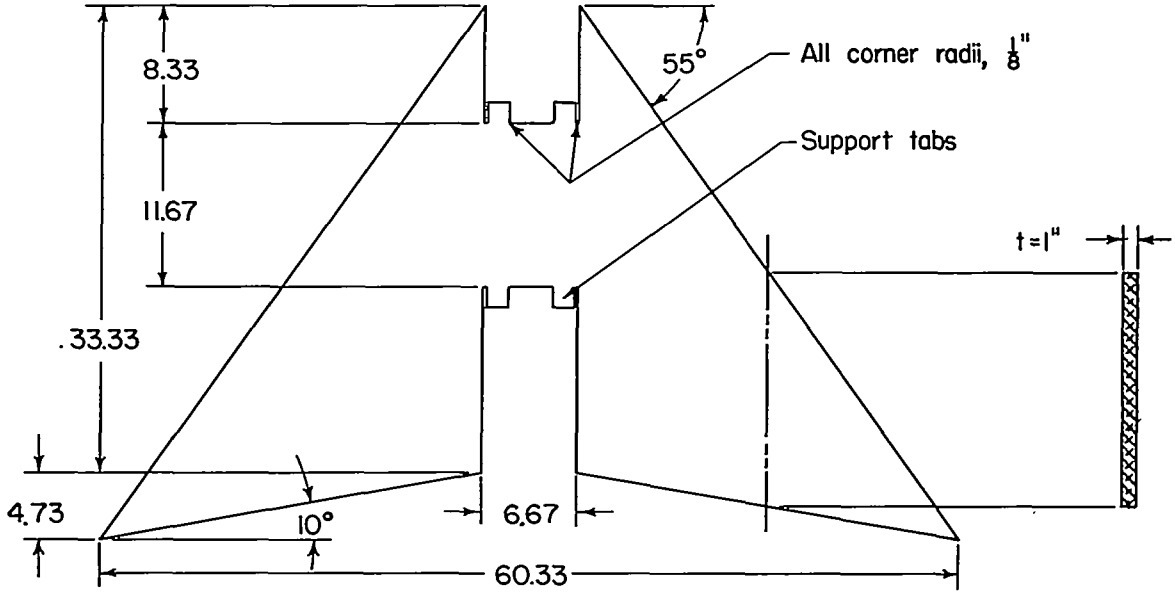

(a) Constant-thickness delta wing.

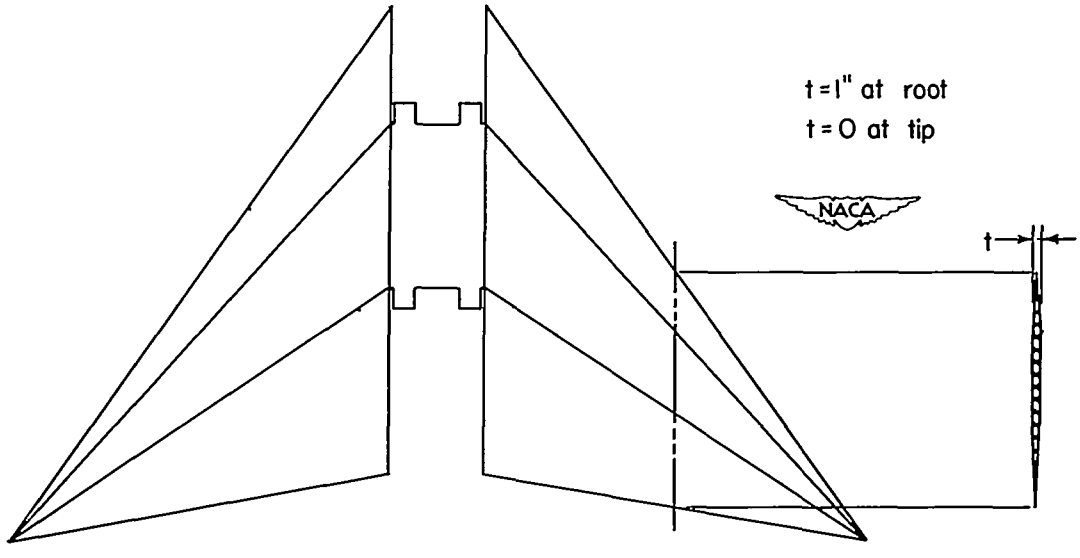

(b) Constant-thickness-ratio delta wing.

Figure 1.- Delta wings having a carry-through-bay chord smaller than the wing root chord. All dimensions are in inches.

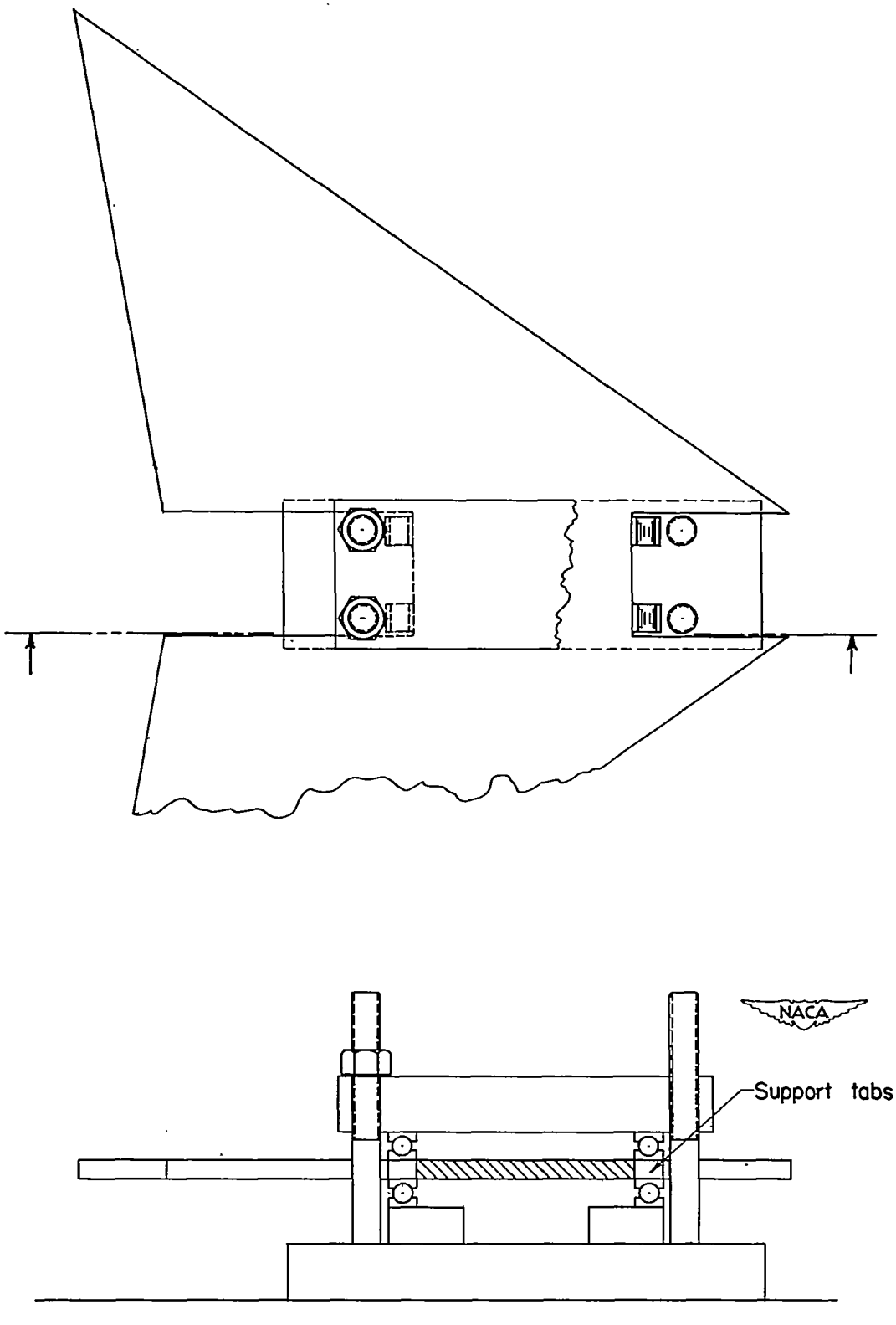

Figure 2.- Method of supporting the delta wings.

NOMINAL COORDINATES OF LOAD AND DEFLECTION STATIONS

Station	Load station		Deflection station	
	x	y	x	y
1	26.0	0.5	26.7	0.1
2	20.1	1.5	20.1	1.3
3	20.1	8.9	20.1	9.4
4	13.4	2.7	13.4	2.5
5	13.4	10.7	13.4	10.4
6	13.4	18.4	13.4	18.9
7	6.7	3.9	6.7	3.7
8	6.7	9.8	6.7	9.5
9	6.7	16.1	6.7	15.8
10	6.7	22.3	6.7	22.0
11	6.7	27.9	6.7	28.4
12	0.4	5.0	0.1	4.9
13	1.0	17.3	1.0	17.0
14	1.0	23.9	1.0	23.6
15	1.0	30.5	1.0	30.2
16	0.4	36.9	0.1	37.8

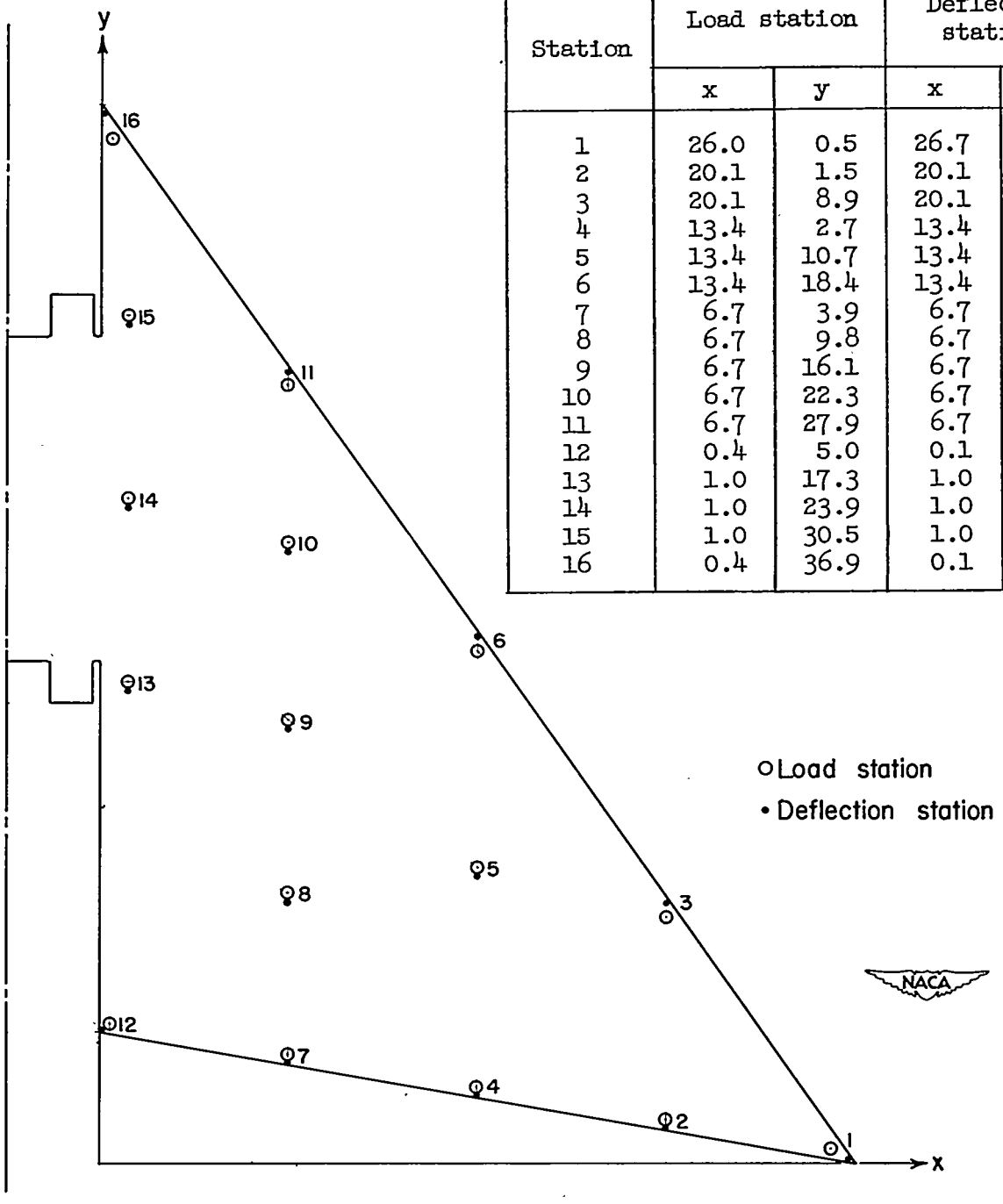

Figure 3.- Location of load and deflection stations.

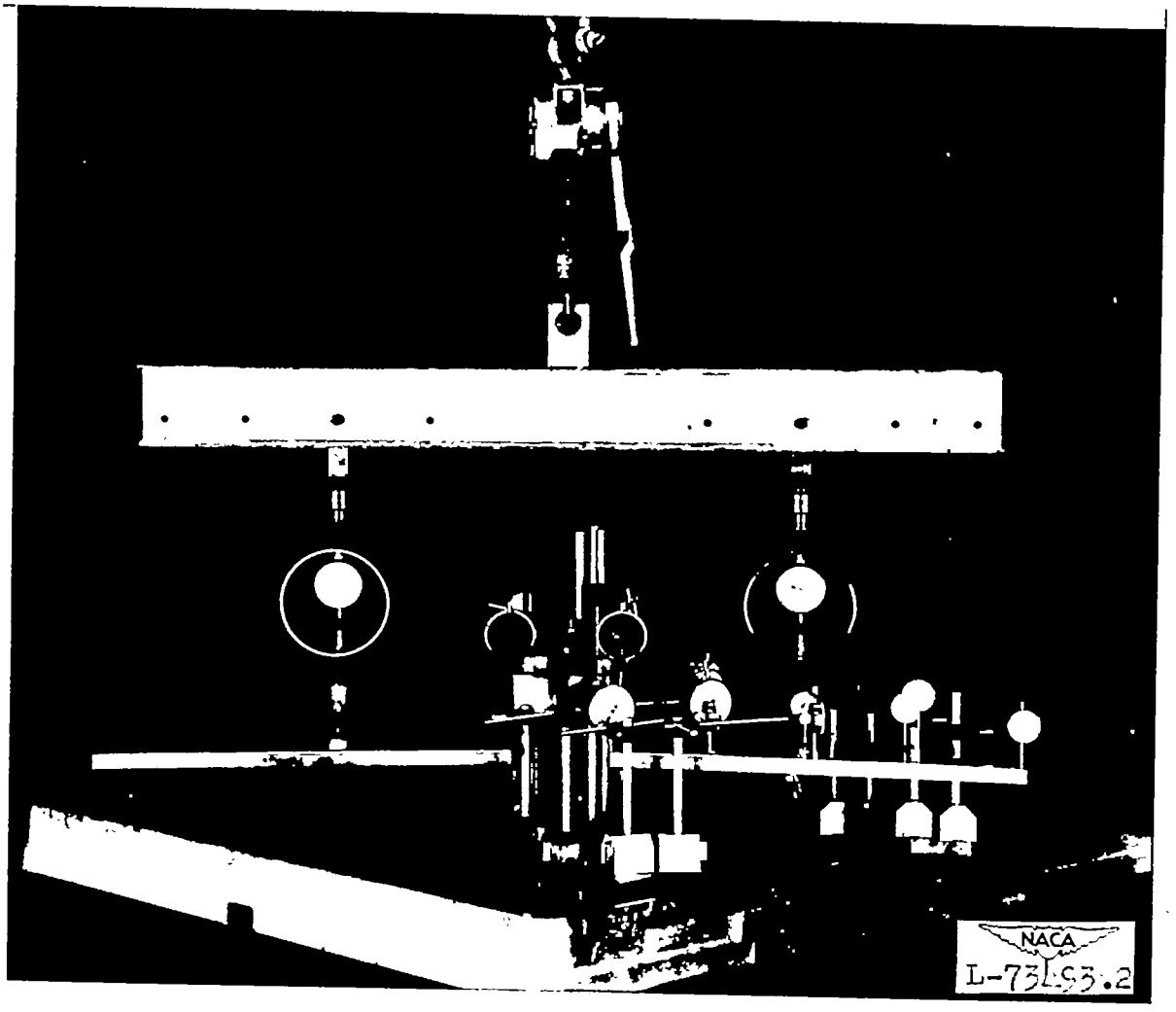

Figure 4.- Test setup.

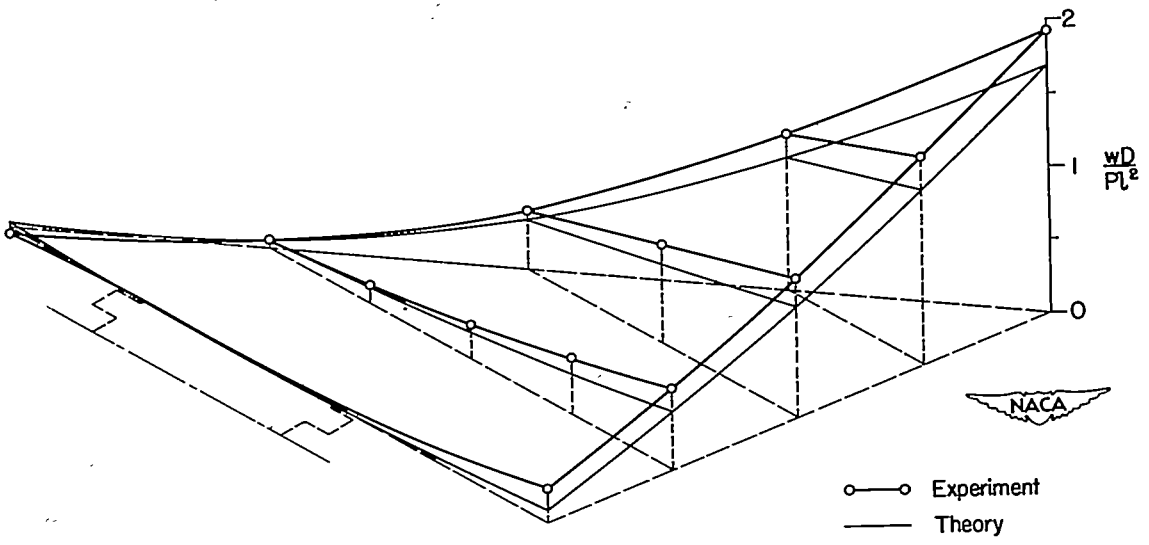

Figure 5.- Comparison of experiment with theory for the tip-load deflections of constant-thickness delta wing.

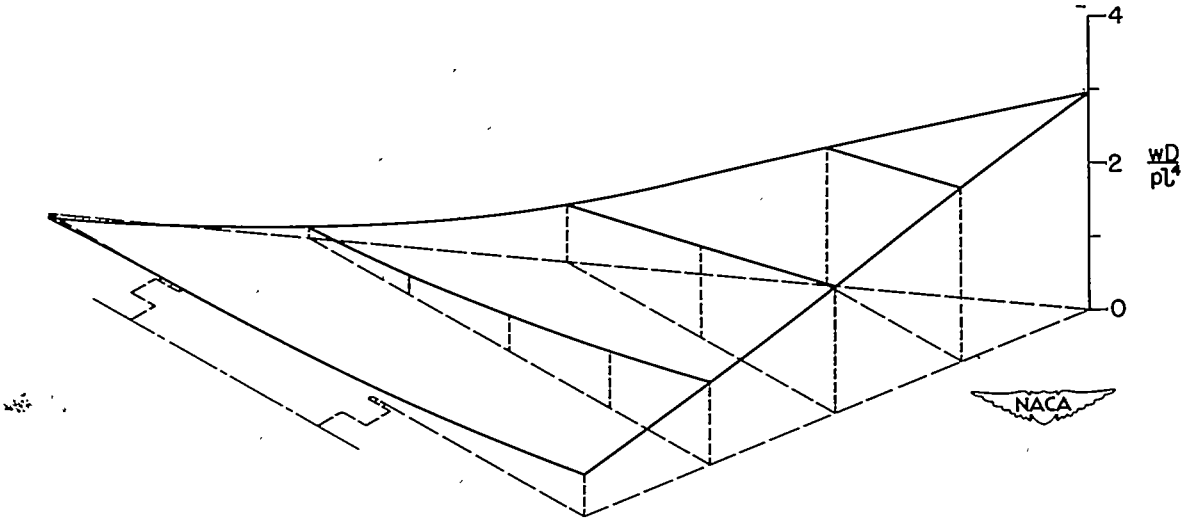

Figure 6.- Uniform-load deflections of constant-thickness delta wing computed from experimental influence coefficients of table 1.

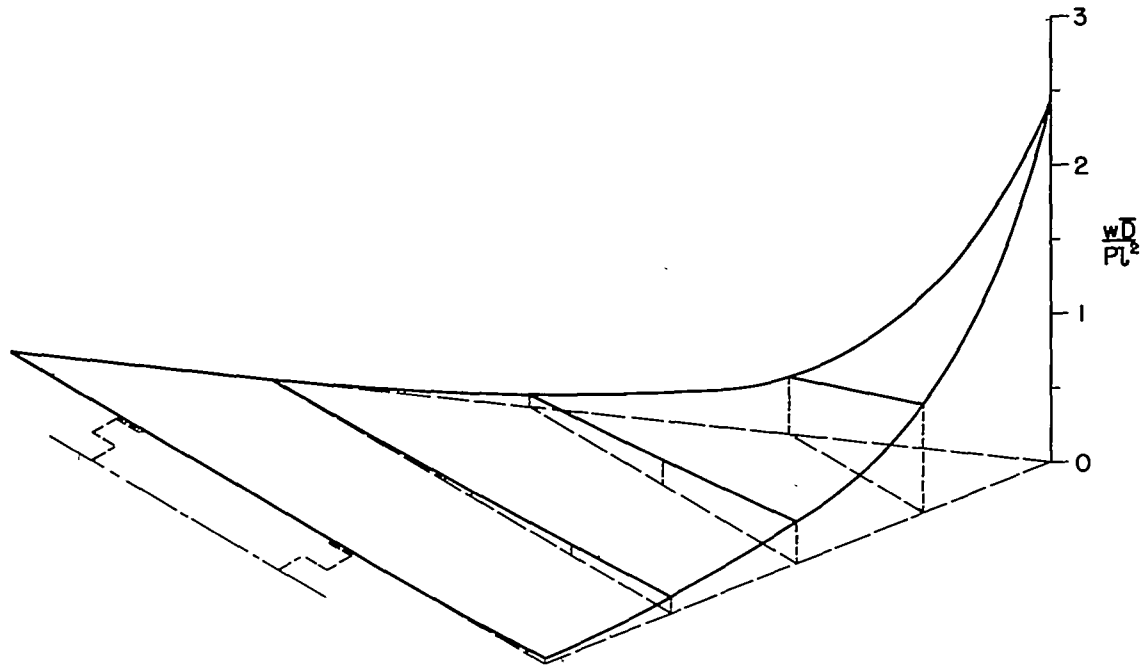

(a) Tip-load deflections.

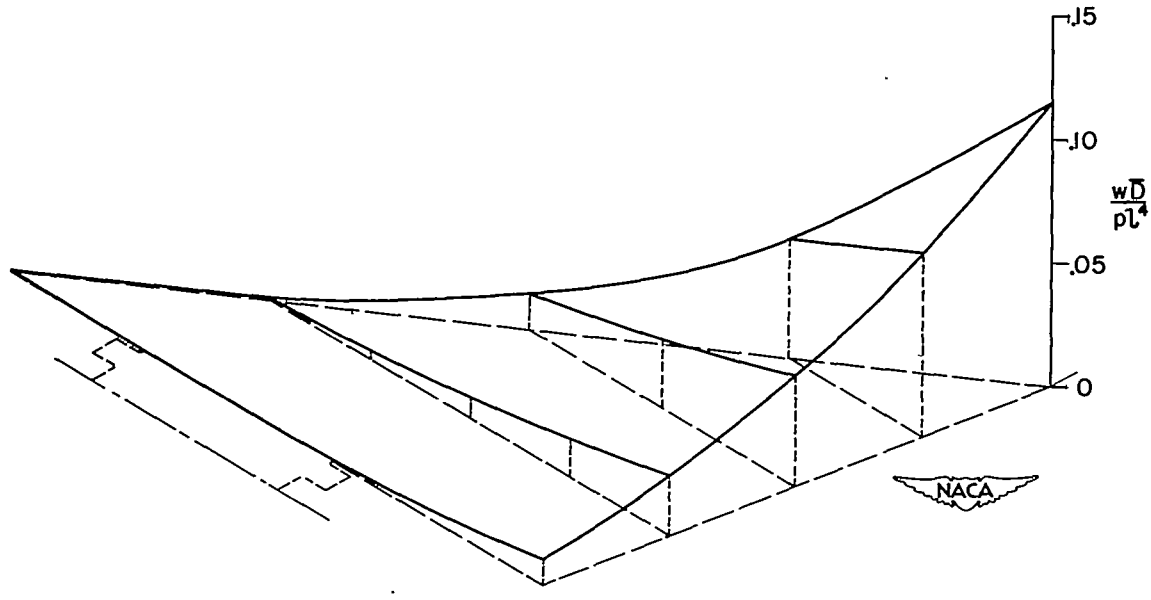

(b) Uniform-load deflections computed from experimental influence coefficients of table 2.

Figure 7.- Deflections obtained from experiments with constant-thickness-ratio delta wing.

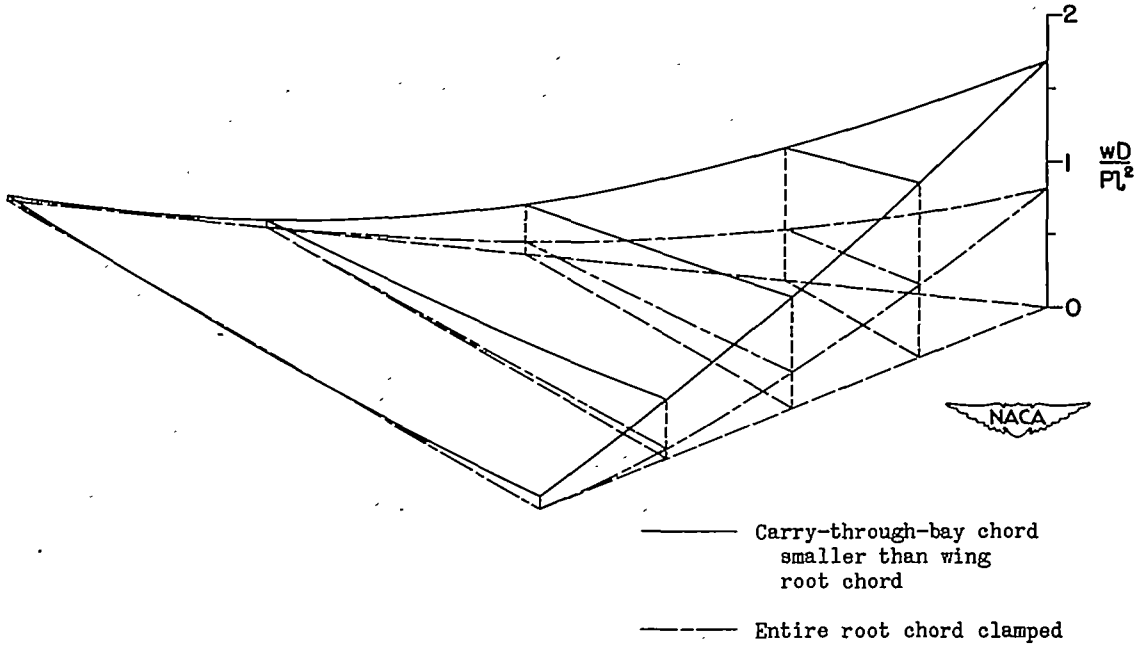

Figure 8.- Comparison of theoretical tip-load deflections of wing having carry-through-bay chord smaller than wing root chord with deflections of wing having entire root chord clamped.

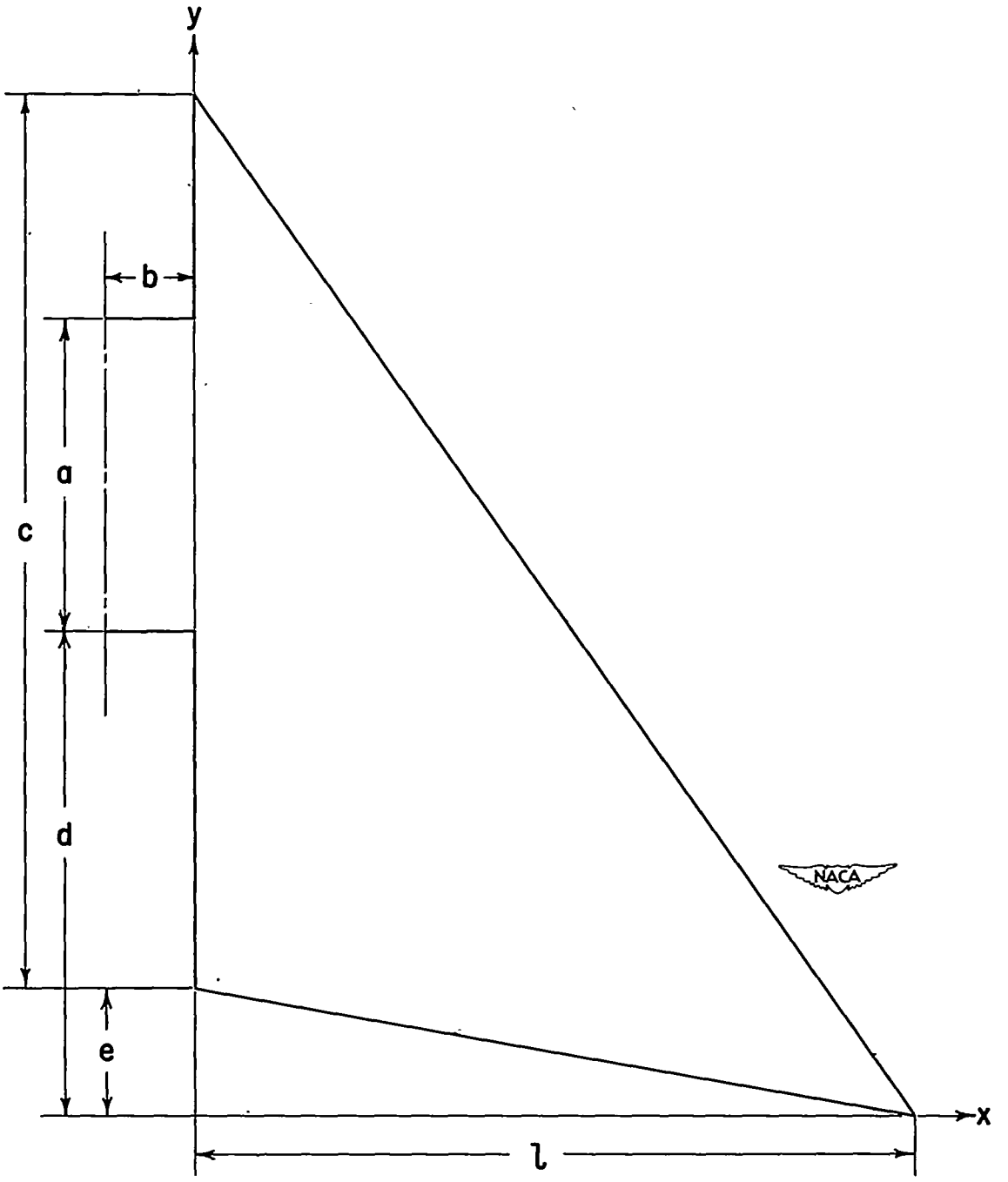

Figure 9.- Coordinate system used in the analysis of the appendix.

NACA-Langley - 5-1-53 - 1000